


Ab initio* valence-space in-medium similarity renormalization group calculations for neutron-rich P, Cl, and K isotopes

M. R. Xie (谢萌冉)^{1,2} L. Y. Shen (沈留媛)^{1,2} J. G. Li (李健国)^{1,2†} H. H. Li (李红蕙)^{1,2}
Q. Yuan (袁琪)^{1,2} W. Zuo (左维)^{1,2} 

¹Institute of Modern Physics, Chinese Academy of Sciences, Lanzhou 730000, China

²School of Nuclear Science and Technology, University of Chinese Academy of Sciences, Beijing 100049, China

Abstract: Neutron-rich P, Cl, and K isotopes, particularly those with neutron numbers of approximately $N = 28$, have attracted extensive experimental and theoretical interest. We utilize the *ab initio* valence-space in-medium similarity renormalization group approach, based on chiral nucleon-nucleon and three-nucleon forces, to investigate the exotic properties of these isotopes. Systematic calculations of the low-lying spectra are performed. A key finding is the level inversion between $3/2_1^+$ and $1/2_1^+$ states in odd- A isotopes, attributed to the inversion of $\pi 0d_{3/2}$ and $\pi 1s_{1/2}$ single-particle states. The *ab initio* calculations, which incorporate the three-nucleon forces, correlate closely with existing experimental data. Further calculations of effective proton single-particle energies provide deeper insights into the shell evolution for $Z = 14$ and 16 sub-shells. Our results indicate that the three-body force plays important roles in the shell evolution for $Z = 14$ and 16 sub-shells with neutron numbers ranging from 20 to 28. Additionally, systematic *ab initio* calculations are conducted for the low-lying spectra of odd-odd nuclei. The results correspond with experimental data and provide new insights for future research into these isotopes up to and beyond the drip line.

Keywords: *ab initio* calculations, shell evolution, low-lying spectra

DOI: 10.1088/1674-1137/ad47aa

I. INTRODUCTION

An atomic nucleus represents a complex quantum many-body system, where neutrons and protons are bound together through strong nuclear interactions. Our comprehension of the nuclear structure is fundamentally anchored in the shell model, a significant theoretical framework that describes the arrangement of nucleons within a nucleus [1, 2]. The discovery of rare isotope beams has revealed that the properties of nuclei with extreme N/Z ratios within the nuclear chart strongly modify to the well-known shell structure [3–6]. Systematic explorations into exotic nuclei have shown that traditional shell gaps are not immutable; rather, they evolve, leading to the disappearance of traditional magic numbers and the emergence of new shell closures [6–11]. Significant shell gaps observed in ^{22}O and ^{24}O suggest new magic numbers at $N = 14$ and 16 , respectively [11–13], with further discoveries of magic numbers at $N = 32, 34$ in Ca isotopes [14–15]. Additionally, the halo phenomenon in ^{11}Li

suggests the disappearance of the $N = 8$ shell closure, and studies on isotopes such as ^{29}F , ^{39}Na , and ^{40}Mg indicate the disappearance of magic numbers at $N = 20$ and 28 [16–22]. These discoveries have not only profoundly increased our understanding of nuclear physics but also challenged pre-existing paradigms of nuclear stability and structures.

Alterations in nuclear shell structures, primarily driven by the monopole interaction, are a focal topic in contemporary nuclear physics research [23–26]. Both experimental and theoretical studies have extensively investigated the monopole shift observed in proton-hole states within neutron-rich isotopes [27–29]. In K isotopes ranging from ^{39}K to ^{47}K , a noteworthy shift in the energy levels between the $1/2_1^+$ and $3/2_1^+$ states is observed, culminating in an inversion at ^{47}K , where the $1/2_1^+$ state becomes the ground state [30–32]. This inversion, particularly evident at $N = 28$, signifies an energy level reversal between the $\pi 0d_{3/2}$ and $\pi 1s_{1/2}$ orbits and highlights the crucial role of tensor forces in these isotopes [23, 33, 34].

Received 21 February 2024; Accepted 26 April 2024; Published online 27 April 2024

* Supported by the National Key R&D Program of China (2023YFA1606403), the National Natural Science Foundation of China (12205340, 12175281, 12347106, 12121005), the Natural Science Foundation of Gansu Province, China (22JR5RA123, 23JRRA614), the Strategic Priority Research Program of Chinese Academy of Sciences (XDB34000000), the Key Research Program of the Chinese Academy of Sciences (XDPB15), the State Key Laboratory of Nuclear Physics and Technology, Peking University (NPT2020KFY13). The numerical calculations in this paper have been done on Hefei advanced computing center

† E-mail: jianguo_li@impcas.ac.cn

©2024 Chinese Physical Society and the Institute of High Energy Physics of the Chinese Academy of Sciences and the Institute of Modern Physics of the Chinese Academy of Sciences and IOP Publishing Ltd

Interestingly, this inversion is not limited to K isotopes. A similar inversion between the $1/2_1^+$ and $3/2_1^+$ states occurs in the Cl isotopic chain [35, 36]. This raises the question: What happens after $N = 28$ for more rich neutrons? Furthermore, recent advancements using γ -ray spectroscopy and exclusive parallel momentum distribution analysis have established a ground state spin $3/2^+$ for ^{51}K and ^{53}K , suggesting that the order of the $\pi 0d_{3/2}$ and $\pi 1s_{1/2}$ orbits returns to normal in the vicinity of $N = 32$ and 34 [28, 29]. Nevertheless, the precise dynamics of energy splitting in neutron-rich P, Cl, and K isotopes close to and beyond the drip line require further investigation.

Our understanding of neutron-rich isotopes of P, Cl, and K is constrained by limited and occasionally contradictory data. For example, our understanding of ^{49}K , characterized by an extensive level scheme with all spins, including in the ground state, remains tentative [37]. Theoretical efforts to describe nuclei in this region have encountered challenges. Notably, large-scale shell model calculations using the SDPF-U phenomenological effective interaction [33] have been employed to describe the properties of these nuclei. Additionally, the *ab initio* Gorkov self-consistent Green's function method has contributed to the understanding of neutron-rich Cl and K isotopes [28, 36, 38]. However, only the $1/2_1^+$ and $3/2_1^+$ states have been mentioned [28, 36, 38]. The *ab initio* valence-space in-medium similarity renormalization group (VS-IMSRG) approach, based on chiral nucleon-nucleon (NN) and three-nucleon ($3N$) interactions, provides a systematic and reliable prediction of nuclear properties [11, 39–42]. The VS-IMSRG has been successfully adopted to describe the properties of nuclei within this region, such as the unique deformation properties of ^{40}Mg and ^{42}Si [42]. Furthermore, VS-IMSRG calculations have revealed $N = 32$ and 34 sub-shell closures, particularly in calcium chains [9, 43–45].

The remainder of this paper is structured as follows: First, we outline the foundational principles of the *ab initio* VS-IMSRG theoretical framework. We then comprehensively analyze the low-lying spectra for odd- A neutron-rich P, Cl, and K isotopes, employing two sets of chiral $NN+3N$ interactions. This analysis reveals the shell evolution across these isotopic chains for neutron numbers ranging from $N = 22$ to 40 , and we utilize effective single-particle energies (ESPEs) to elucidate nuclear shell evolutions. Subsequently, the spectra of these neutron-rich isotopes of odd-odd nuclei are predicted, with our results remaining open to future experimental validation. Finally, a summary of the article is given.

II. METHOD

The intrinsic Hamiltonian for an A -nucleon system is formulated as

$$H = \sum_{i<j}^A \left(\frac{(\mathbf{p}_i - \mathbf{p}_j)^2}{2mA} + v_{ij}^{NN} \right) + \sum_{i<j<k}^A v_{ijk}^{3N}, \quad (1)$$

where \mathbf{p} is the momentum of nucleons in the laboratory, m is the nucleon mass, and v^{NN} and v^{3N} are the NN and $3N$ interactions, respectively. The Hamiltonian, initially expressed in terms of nucleon momentum and interactions, is reformulated using normal-ordered operators, predominantly truncated at the two-body level. This reformulation ingeniously incorporates the $3N$ interaction effects within the two-body framework, streamlining the computational complexity.

In this study, we employ two sets of $NN+3N$ chiral forces, *i.e.*, EM1.8/2.0 [46, 47] and $NN+3N(\text{Inl})$ interactions [38]. The EM1.8/2.0 interaction is composed of a next-to-next-to-next-to-leading order ($N^3\text{LO}$) NN interaction [48] softened by the similarity renormalization group (SRG) evolution with a momentum resolution scale of $\lambda = 1.8 \text{ fm}^{-1}$ and a next-to-next-to-leading order ($N^2\text{LO}$) nonrenormalized three-nucleon force (3NF) with a momentum cutoff of $\Lambda = 2.0 \text{ fm}^{-1}$. The 3NF is fitted to the ^3H binding energy and ^4He charge radius based on the softened SRG $\lambda = 1.8 \text{ fm}^{-1}$ NN interaction [46, 47]. The $NN+3N(\text{Inl})$ interaction incorporates both local and nonlocal $3N$ regulators (Inl) and refits $3N$ parameters for $A = 2, 3, 4$ nuclei based on the bare $N^3\text{LO}$ NN potential [38]. In this study, we adopt a large SRG scale of $\lambda = 2.6 \text{ fm}^{-1}$ for the NN interaction [48] and neglect the induced 3NF . For the $3N$ part of the $NN+3N(\text{Inl})$ interaction, the bare interaction is adopted in the actual calculations. These interactions accurately reproduce the ground state energies and predict drip lines in light to medium mass nuclei, which have been extensively validated for various isotopic chains [47, 49–51]. Our computational analysis is executed within a spherical harmonic-oscillator basis including up to $e_{\text{max}} = 2n + l = 14$ and limits the three-body matrix elements to $E_{3\text{max}} = 14$. The oscillator frequency of $\hbar\omega$ is fixed at 16 MeV .

The VS-IMSRG is used to decouple the normal-ordered Hamiltonian from the large Hilbert space to a small valence space. This is achieved by solving the flow equation,

$$\frac{dH(s)}{ds} = [\eta(s), H(s)], \quad (2)$$

with an anti-Hermitian generator,

$$\eta(s) \equiv \frac{dU(s)}{ds} U^\dagger(s) = -\eta^\dagger(s). \quad (3)$$

The Magnus formulation of the VS-IMSRG [39, 52] is adopted to construct an approximate unitary transformation to decouple the ^{28}O core. Subsequently, we con-

struct a valence-space Hamiltonian for valence protons in the *sd* shell and valence neutrons in the *pf* shell, effectively reducing the complexity of the full *A*-body problem. In our previous study [42], we employed the valence space Hamiltonian to study the deformations in ^{40}Mg , ^{42}Si , and ^{44}S $N = 28$ isotones, which agreed well with the experimental data. This approach is refined using the ensemble normal-ordering (ENO) technique detailed in Ref. [53]. The VS-IMSRG code of Ref. [54] is utilized for that matter. In practical calculations, the Magnus formalism is employed with all operators truncated at the two-body level [52]. Finally, we employ the KSHELL shell-model code [55] for the final diagonalization of valence space Hamiltonians.

III. RESULTS

Spectroscopic studies of odd-*A* and odd-odd nuclei are critical in validating single-particle structures and refining theoretical models. Neutron-rich P, Cl, and K isotopes, featuring proton holes in the *sd* shell, are of particular interest to elucidate single-particle structures in this notable region of the nuclide chart. Our study begins with calculations of the energy spectrum for odd-*A* nuclear isotopes with the VS-IMSRG using two sets of $NN + 3N$ chiral interaction, *i.e.*, $NN + 3N$ (Inl) and EM1.8/2.0 interactions. Before discussing the results of energy spectrum calculations, we assess the effect of the 3NF on the low-lying energy spectra using ^{47}K as an example. We compare the results of calculations using the $NN + 3N$ (Inl) interaction without the inclusion of the 3NF (labeled NN), the full $NN + 3N$ (Inl) interaction, the EM1.8/2.0 interaction, and the available experimental data [56]. The results are presented in Fig. 1. The calculated ground state without the 3NF exhibits significant discrepancies compared to the experimental data. The incorporation of the 3NF into the VS-IMSRG calculations significantly enhances the consistency of the calculated results with the experimental data. This comparison clearly underscores the importance of including the 3NF in energy spectrum calculations and validates the significant contribution of the 3NF in enhancing the accuracy of spectral calculations.

In the following calculations, we present only the results considering the 3NF. The results of low-lying spectra of the neutron-rich odd-*A* P, Cl, and K isotopes are shown in Figs. 2, 3, and 4, respectively. Moreover, the available experimental data are shown for comparison.

The ground state spin and parity of odd-*A* nuclei can reflect the primary configuration of the last odd nucleon within the shell model framework. In the neutron-rich P isotopes, the shell model traditionally predicts a $1/2^+$ ground state, corresponding to the last odd proton occupying the $\pi 1s_{1/2}$ orbit under normal orbital ordering. Our *ab initio* VS-IMSRG calculations, utilizing two sets

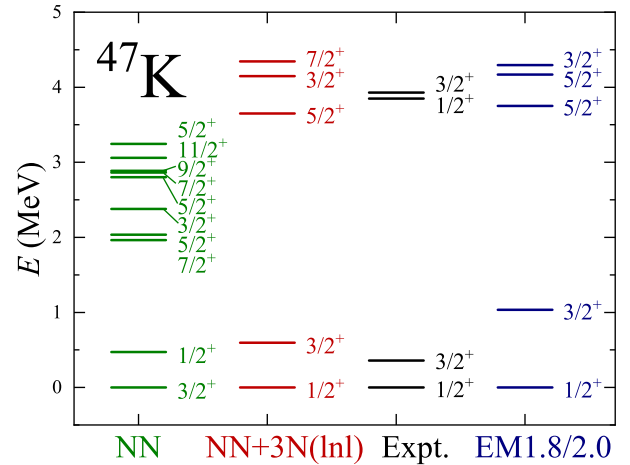


Fig. 1. (color online) Calculated spectra of ^{47}K with and without the 3NF for the $NN + 3N$ (Inl) interaction, along with experimental data [56] and results from the EM1.8/2.0 $NN + 3N$ interaction.

of $NN + 3N$ interactions, agree well with the available experimental data, particularly for the low-lying states of ^{39}P , where both interactions align closely with the experimental data [58]. Notably, results from the $NN + 3N$ (Inl) and EM1.8/2.0 interactions are nearly identical, with the notable exception of the low-lying states of ^{43}P , where the EM1.8/2.0 interaction predicts a $3/2^+$ ground state, in contrast to the experimental value of $1/2^+$ [58]. The experimental data on the low-lying states of the neutron-rich P isotopes remain sparse, yet both our calculations and available experimental evidence, except for ^{43}P using the EM1.8/2.0 potential, consistently indicate a $1/2^+$ ground state for odd-*A* $^{37-45}\text{P}$ isotopes. However, the energy level splitting between $E(1/2^+)$ and $E(3/2^+)$ decreases from ^{37}P to ^{45}P . Similar results are obtained in large-scale shell model calculations [63]. Both two $NN + 3N$ interactions predict that the ground state of ^{45}P is $1/2^+$, whereas experimental data are lacking.

Extending the analysis to Cl ($Z = 17$) isotopes, a notable uncertainty surrounds the energy spectrum, particularly in isotopes such as $^{41,43,45,47}\text{Cl}$. Neutron-rich Cl isotopes are of particular interest because the experimental data suggest that energy levels of $1/2^+$ and $3/2^+$ states initially reverse with increasing neutron number and then return to the natural order. As shown in Fig. 3, the predictions of the energy order of the low excited states of the Cl isotopes by both interactions are almost identical, except for ^{41}Cl . Note that ^{39}Cl with $N = 22$ exhibits the expected spin-parity with a $3/2^+$ ground state. However, this changes in ^{41}Cl , where a $1/2^+$ ground state is favored [61, 64, 65]. This inference is obtained from observed decay patterns in lighter isotopes, where the yrast $5/2^+$ level predominantly decays to the $3/2^+$ state, seldom to the $1/2^+$ level. Support for a $1/2^+$ assignment in ^{41}Cl also comes from the β -decay of ^{41}S [66]. The results corres-

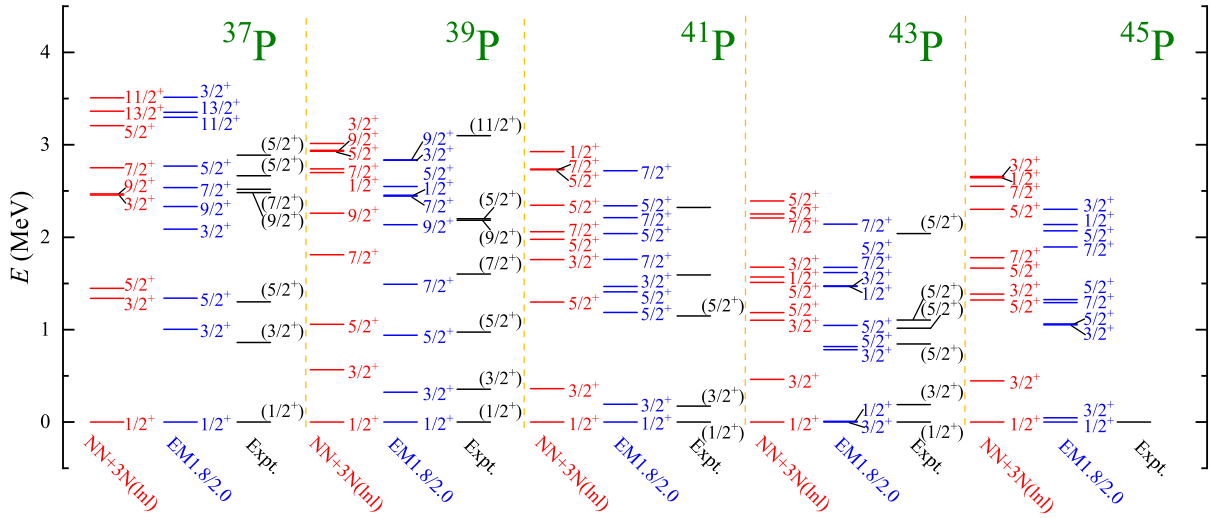


Fig. 2. (color online) Calculated spectra of the odd- A P isotopes using the *ab initio* VS-IMSRG for chiral $NN+3N$ (1nl) and EM1.8/2.0 interactions, along with available experimental data [57, 58].

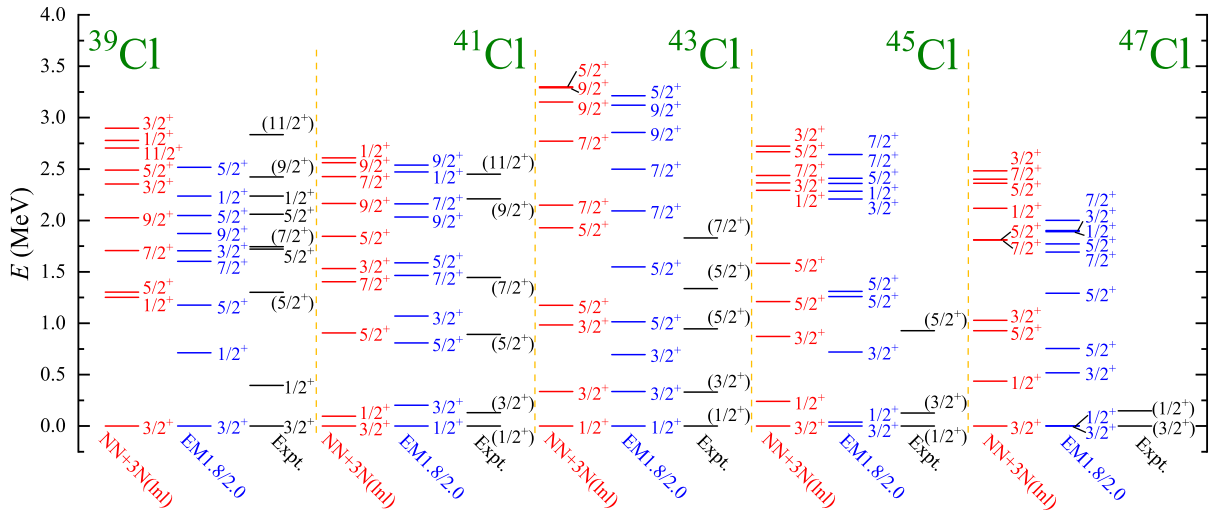


Fig. 3. (color online) Similar to Fig. 2, but for neutron-rich odd- A Cl isotopes. Experimental data are obtained from Refs. [57, 59–61].

pond with the VS-IMSRG calculations using the EM1.8/2.0 interaction. For ^{45}Cl , the experimental data of Ref. [67] have suggested that the ground state is $1/2_1^+$, while recent studies suggest a shift toward a $3/2_1^+$ ground state [59]. The new results with $3/2_1^+$ ground state for ^{45}Cl are consistent with our VS-IMSRG calculations with both sets of $NN+3N$ interactions. Similarly, for ^{43}Cl , robust evidence from in-beam γ spectroscopy after fragmentation strongly indicates an inverted $1/2_1^+$ ground state [67], which also corresponds with the VS-IMSRG predictions. Moreover, our VS-IMSRG calculations reproduce the experimental $3/2_1^+$ and $1/2_1^+$ energy splitting gaps well. Note that the energy level order of ^{43}Cl predicted using the VS-IMSRG agrees with the experimental data. In addition, the VS-IMSRG predicts a $3/2_1^+$ ground state for ^{47}Cl , consistent with the experimental results in Ref. [59].

Neutron-rich K isotopes have attracted considerable interest both experimentally and theoretically [37, 68–70]. For K isotopes, the calculations with the $NN+3N$ (1nl) and EM1.8/2.0 interactions closely produce the energy level of low-lying states, and the results agree with the experimental data. For example, the predicted excitation energies for the $5/2_1^+$ state for ^{49}K agree well with experimental evidence. Furthermore, a potential undetected $3/2_2^+$ state lying above it is suggested in our *ab initio* calculations, which is missed in experiments. The inversion and restoration of the ground state spin-parity also occur in K isotopes as the neutron number increases up to $N=40$. Experiments have confirmed that the ground state of $^{47,49}\text{K}$ is $1/2_1^+$ [29, 32, 37], and it changes to $3/2_1^+$ in nearby odd- A K isotopes. Our *ab initio* VS-IMSRG calculations using both $NN+3N$ (1nl) and EM1.8/2.0

interactions agree well with the experimental data, particularly the ground state spin-parities and energy splittings of the $3/2_1^+$ and $1/2_1^+$ states for K isotopes. The large-scale shell model calculations with SDPF-NR interaction predict the ground state of ^{49}K as $1/2^+$, while the calculations with SDPF-U and SDPF-MU interactions predict a $3/2^+$ ground state [29]. Our *ab initio* calculations with both sets of $NN+3N$ interactions indicate a ground state of ^{49}K as $1/2^+$. Additionally, higher excited states are predicted by our calculations for the neutron-rich odd- A P, Cl, and K isotopes, which will offer insights for future experimental endeavors.

The variation in ESPEs as a function of neutron number N or proton number Z is crucial for understanding shell evolution, as emphasized in Refs. [6, 23]. Shell model calculations have highlighted the importance of central and tensor forces in altering the $N=20$ and $N=28$ shell gaps, particularly noting the significant impact of tensor forces on the energy shift of spin-orbit partners [6, 25]. The evolution for the $3/2_1^+$ and $1/2_1^+$ states in the neutron-rich odd- A P, Cl, and K isotopes is of particular interest for understanding the nuclear structure, which is attributed to the evolution of $\pi 0d_{3/2}$ and $\pi 1s_{1/2}$ single-particle states. To elucidate the shell evolution in the neutron-rich P, Cl, and K isotopes, we comprehensively analyze the ESPEs for the proton single particle state based on the effective valence-space Hamiltonian derived from the VS-IMSRG.

The calculated ESPEs are depicted in Fig. 5. The energy gap of $\pi 0d_{5/2}$ and $\pi 1s_{1/2}$ relative to $\pi 0d_{3/2}$ single-particle states is presented, which can reveal significant shifts in orbital energy splitting as N increases. Specifically, the neutron-rich P, Cl, and K isotopes exhibit nearly identical variations in the orbital gaps between $\pi 0d_{3/2}$ and $\pi 0d_{5/2}$ across the neutron numbers $N=22-40$. Further-

more, the gaps between the $\pi 1s_{1/2}$ and $\pi 0d_{3/2}$ orbits display a similar pattern in the neutron-rich P, Cl, and K isotopes. They initially decrease and then increase with the addition of neutrons, stabilizing once at $N \geq 32$. Shell model calculations have suggested that the decrease in the shell gap between $\pi 1s_{1/2}$ and $\pi 0d_{3/2}$ is mainly affected by the tensor force [71]. It is important to note that around $N=28$, the energies of the $\pi 0d_{3/2}$ and $\pi 1s_{1/2}$ orbits are nearly degenerate, which form a pseudo- $SU3$ doublet that enhances the quadrupole correlations of the configurations with open-shell neutrons [33]. Notably, beyond $N=28$, the shell gap increases, regaining its standard order. Furthermore, our VS-IMSRG calculations are compared to the results from the Gorkov-Green's functions theory [72] and shell model calculations with SDPF-MU interaction. In the Gorkov-Green's functions theory, the ESPEs of $\pi 0d_{3/2}$ and $\pi 1s_{1/2}$ recall the fragmented $3/2^+$ and $1/2^+$ strengths derived from one-proton addition and removal processes on neighboring Ca isotones [73]. This comparison reveals a consistency in the evolutionary trends of ESPEs predicted using the VS-IMSRG and Gorkov-Green's function theory, particularly beyond $N=26$. Compared to the shell model results, derived from the Ca isotope chain, both methods indicate the disappearance of magic number $Z=16$ at $N=28$. Notably, beyond $N=28$, the shell model results closely correspond with those obtained using the EM1.8/2.0 interaction.

Note that the EM1.8/2.0 interaction produces $\pi 0d_{3/2}$ and $\pi 1s_{1/2}$ orbits that are inverted at $N=28$, with a crossover in the ESPEs in the neutron-rich Cl and K isotopes. However, the VS-IMSRG predicts the ^{45}Cl ground state to be $3/2^+$. Although the ESPE provides a preliminary framework for nuclear energy levels, the interactions between nucleons and the collective effects resulting

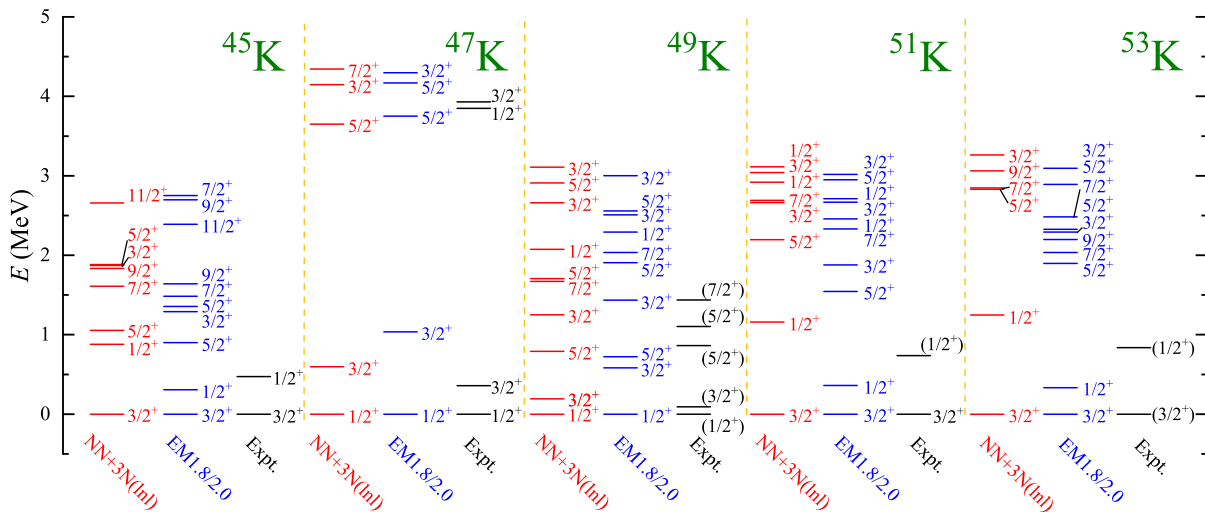


Fig. 4. (color online) Similar to Fig. 2, but for neutron-rich odd- A K isotopes. Experimental data are obtained from Refs. [28, 37, 56, 57, 62].

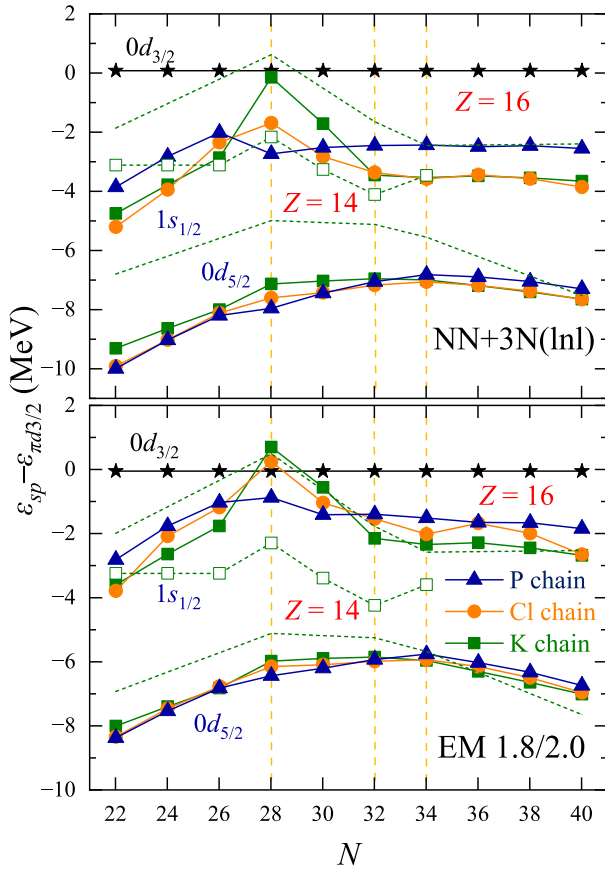


Fig. 5. (color online) ESPEs of the $\pi 0d_{3/2}$, $\pi 1s_{1/2}$, and $\pi 0d_{5/2}$ orbits in P, Cl, and K isotopes for $N = 22 - 40$, calculated using $NN + 3N(\ln l)$ and EM1.8/2.0 interactions (dashed lines). Furthermore, the calculated ESPEs for K isotopes from the Gorkov-Green's functions theory (green blank square dotted lines) and the shell model with SDPF-MU interaction (green dotted lines), as reported in Refs. [72, 71] are shown for comparison.

from them play a decisive role in the actual occupation and formation of the ground state of the nucleus [25]. Interestingly, although the $NN + 3N(\ln l)$ calculations do not exhibit a crossover between the $\pi 1s_{1/2}$ and $\pi 0d_{3/2}$ orbits for the neutron-rich P, Cl, and K isotopes, the VS-IMSRG calculations correctly predict the experimental energy level inversion at ^{47}K and ^{51}K for K isotopes and at ^{41}Cl for Cl isotopes. Notably, the calculated ESPEs clearly show the evolution of proton shells, in which the $Z = 14$ sub-shell exists, whereas the $Z = 16$ shell disappears in the neutron-rich P, Cl, and K isotopes in the vicinity of $N = 28$.

For the 3NF, this analysis shows its contributions to shell evolution. Figure 6 (a) depicts the ESPE of the K isotope chain for $N = 20 - 28$ with and without the 3NF for the $NN + 3N(\ln l)$ interaction. Considering only the NN interaction, a pronounced energy gap exists between the $0d_{3/2}$ and $1s_{1/2}$ orbits, preserving the sub-shell at

$Z = 16$, which contradicts the ground-state level inversion observed in ^{47}K [56]. This implies that the calculations relying solely on the NN interaction are insufficient to account for the shell evolution, particularly for the disappearance of the magic number at $Z = 16$. Conversely, incorporating the 3NF addresses this limitation by elevating the ESPEs. As the neutron number increases, the energy gap at $Z = 16$ diminishes, establishing the foundation for the disappearance of the shell structure at $N = 28$ and underscoring the importance of the 3NF in describing shell evolution. Moreover, through the application of the spin-tensor decomposition method [25, 71, 74], we can isolate different components of the effective NN interaction, facilitating a qualitative analysis of contributions of specific components to the evolution of the ESPE. Figure 6 (b) compares the calculated ESPEs with and without considering tensor forces based on the effective Hamiltonian derived from the $NN + 3N(\ln l)$ interaction. The $0d_{5/2}$ orbit is more significantly impacted by tensor forces compared to the $1s_{1/2}$ orbit, highlighting the significant influence of tensor forces on spin-orbit splitting. When tensor forces are considered, the $0d_{3/2}$ and $1s_{1/2}$ orbits become almost degenerate at $N = 28$, with an energy gap of only 0.228 MeV. This suggests the disappearance of the magic number at $Z = 16$ and agrees with the energy spectra results. The omission of tensor forces results in an increased shell gap between the $0d_{5/2}$ and $1s_{1/2}$ orbits up to 2 MeV, emphasizing the influence of tensor forces on shell evolution. Similar scenarios occur in the P and Cl isotopes, in which the 3NF and tensor forces play important roles in shell evolution.

Furthermore, a significant decrease in the energy gap of the $1s_{1/2}$ and $0d_{3/2}$ orbits at $N = 28$ is observed in the K isotopes, as shown in Fig. 6 (a), which is absent in the same calculations with only NN interactions. Moreover, the influence of tensor forces for the significant decrease in the energy gap is considered negligible, as depicted in Fig. 6 (b). To further understand the mechanism, we calculate the average occupations of valence nucleons for the K isotopes with and without 3N forces, as presented in Table 1. These results show that as the neutron number increases, the valence neutrons sequentially fill the $\nu 0f_{7/2}$ orbit in K isotopes. Notably, at $N = 28$, a sudden increase occurs in the occupancy of the $\pi 0d_{3/2}$ orbit, accompanied by a concurrent decrease in occupancy for the $\pi 1s_{1/2}$ orbit. The attraction of the $\nu 0f_{7/2}$ orbit toward both the $\pi 0d_{3/2}$ and $\pi 1s_{1/2}$ orbits implies that the enhanced occupancy of the $\pi 0d_{3/2}$ orbit results in a more pronounced reduction in its energy compared to the $\pi 1s_{1/2}$ orbit, leading to the degeneracy of the $\pi 0d_{3/2}$ and $\pi 1s_{1/2}$ orbits and a significant decrease in the energy gap of the $1s_{1/2}$ and $0d_{3/2}$ orbits.

The above calculations show that the *ab initio* VS-IMSRG approach provides good descriptions for the odd- A nuclear energy spectrum, and the shell evolution can be

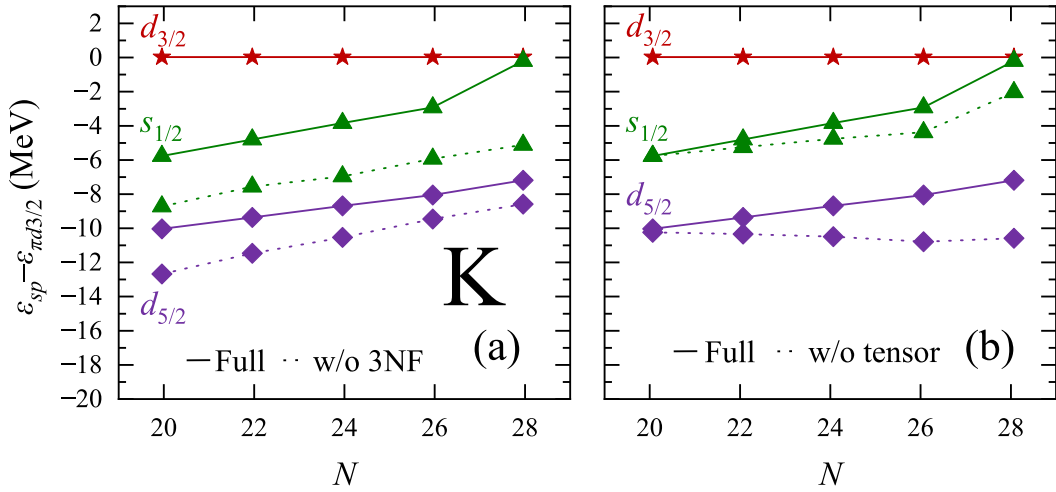


Fig. 6. (color online) Calculations of ESPEs for K isotope chains utilizing the $NN+3N$ (Inl) interaction: (a) Cases with and without the 3NF; (b) comparison of the calculations with and without tensor forces.

Table 1. Calculated average occupancies of valence nucleons for K isotope using only NN and $NN+3N$ (Inl) interactions.

	$\pi 0d_{5/2}$		$\pi 0d_{3/2}$		$\pi 1s_{1/2}$		$\nu 0f_{7/2}$		$\nu 0f_{5/2}$		$\nu 1p_{3/2}$		$\nu 1p_{1/2}$	
	$NN+3N$	NN	$NN+3N$	NN	$NN+3N$	NN	$NN+3N$	NN	$NN+3N$	NN	$NN+3N$	NN	$NN+3N$	NN
^{41}K	5.994	5.999	3.028	3.040	1.978	1.962	1.894	1.982	0.034	0.005	0.063	0.011	0.010	0.002
^{43}K	5.961	5.985	3.074	3.025	1.965	1.990	3.784	3.491	0.082	0.050	0.117	0.437	0.017	0.023
^{45}K	5.952	5.982	3.076	3.065	1.972	1.952	5.653	5.348	0.128	0.087	0.195	0.533	0.024	0.032
^{47}K	5.973	5.992	3.777	3.118	1.250	1.890	7.485	6.942	0.112	0.115	0.377	0.886	0.027	0.058

adequately explained using the ESPE based on the effective valence space Hamiltonian derived from the VS-IMSRG using the EM1.8/2.0 and $NN+3N$ (Inl) interactions. Descriptions of odd-odd nuclei have shown that they are more sensitive to interactions [75]. We extend our analysis to the energy spectrum of odd-odd nuclei. For the P isotopes in Fig. 7, limited experimental data pose a challenge. Nonetheless, our *ab initio* calculations show consistency with the available experimental data for ^{38}P and ^{40}P , which also correspond with large-scale shell model calculations using SDPF-MU interactions [58]. No experimental data of low-lying state information of $^{42,44,46}\text{P}$ have been reported. The predicted level scheme for $^{42,44,46}\text{P}$ is shown and both interactions suggest a 0^- for the ground states, with experimental confirmation required to validate these theoretical predictions. For the Cl isotopes in Fig. 8, the VS-IMSRG calculations well reproduce the low excitation spectrum of ^{38}Cl and hint at the possible presence of an undetected 2^- state in ^{40}Cl . For $^{42,44,46}\text{Cl}$ isotopes, experiments have suggested that their ground states are 2^- [59, 61, 76]. VS-IMSRG calculations for the ground state of ^{44}Cl are consistent with the results in Ref. [59], whereas our VS-IMSRG calculations with both interactions predict that the ground state of ^{42}Cl is 3^- . For ^{46}Cl , our *ab initio* calculations with the $NN+3N$ (Inl) interaction and shell model calculations

with the EPQQM interaction [35] yield a ground state of 0^- , whereas *ab initio* calculations with the EM1.8/2.0 interaction and large-scale shell model calculations with the SDPF-U interaction yield a ground state of 2^- [35]. The discrepancy in the predictions for the spin-parity of the ^{46}Cl ground state underscores the urgent need for definitive experimental evidence.

For odd-odd K isotopes, as depicted in Fig. 9, experimental studies have firmly established the ground state of ^{44}K as 2^- [77, 78]. This experimental determination agrees with our predictions from both EM1.8/2.0 and $NN+3N$ (Inl) interactions, which accurately depict the ground and low-lying excited states. Theoretical calculations suggest that the ground state of ^{46}K is also 2^- and primarily dominated by the $\pi(0d_{3/2})^{-1}\nu(0f_{7/2})^{-1}$ configuration; the results are consistent with those in Ref. [79]. The two interactions offer differing predictions for the ground state of ^{48}K . The ground state predicted from $NN+3N$ (Inl) is 1^- , which is consistent with the suggested ground states in Ref. [80], whereas the calculations with EM1.8/2.0 give a ground state of 2^- . The ground state of ^{50}K and ^{52}K remains experimentally unconfirmed, highlighting a critical area for future research to validate our current understanding of nuclear forces. Moreover, the excited states are predicted in our *ab initio* VS-IMSRG calculations, which may provide a basis for future experi-

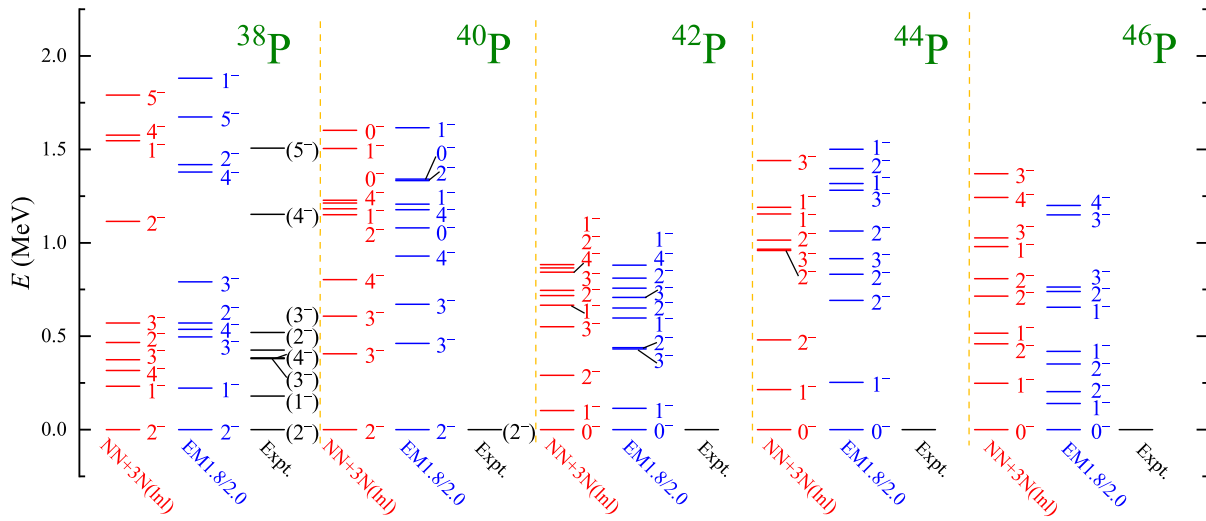


Fig. 7. (color online) Spectra of the even-P isotopes calculated using $NN+3N(\text{lnl})$ and EM1.8/2.0 interactions, with experimental data obtained from Refs. [57, 58].

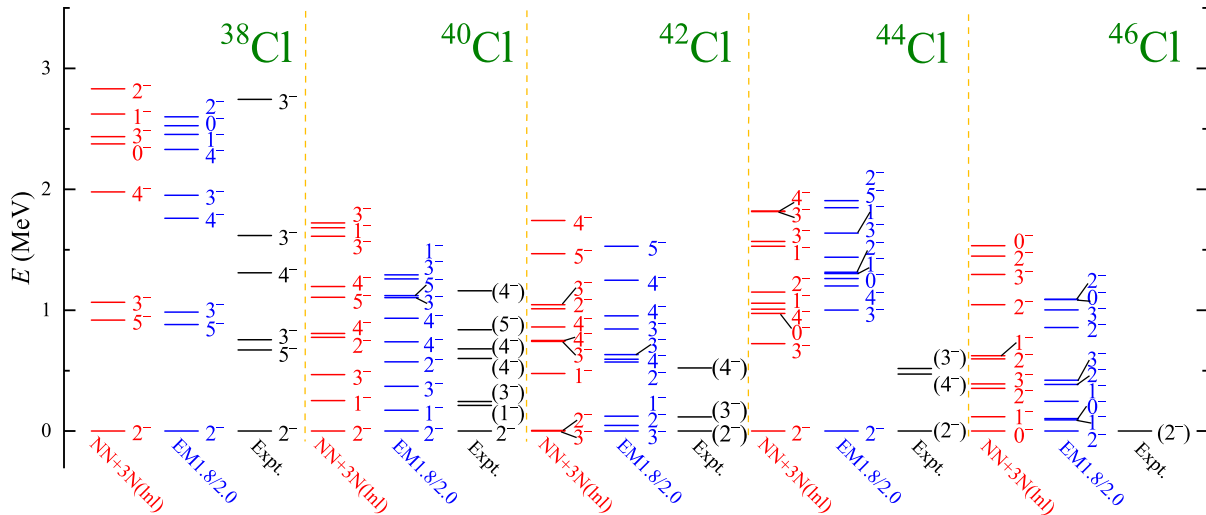


Fig. 8. (color online) Similar to Fig. 7, but for neutron-rich even-Cl isotopes. Experimental data are obtained from Refs. [57, 59, 61, 65].

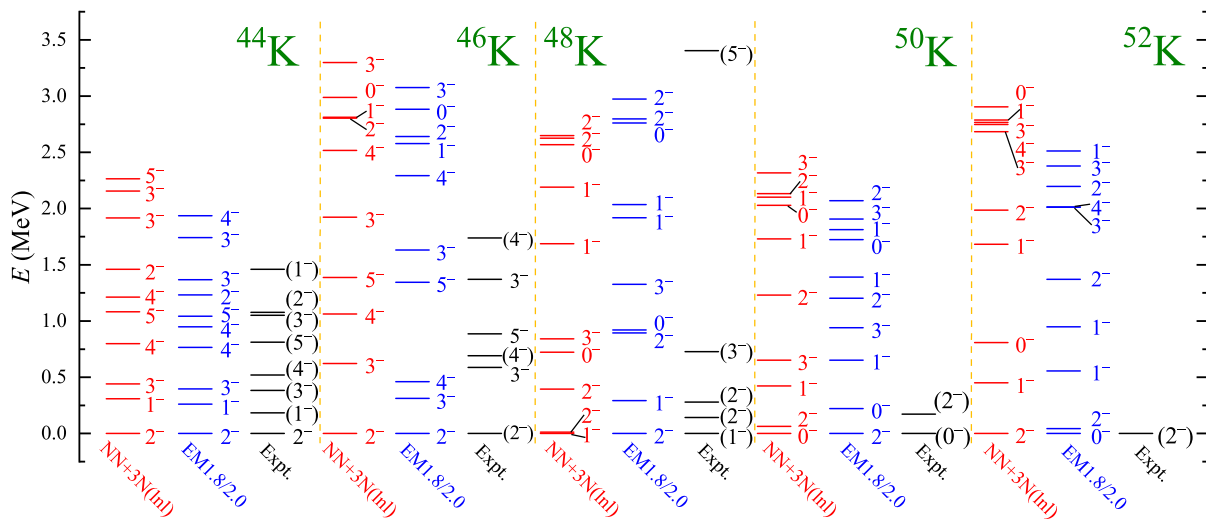


Fig. 9. (color online) Similar to Fig. 7, but for neutron-rich even-K isotopes. Experimental data are obtained from Refs. [57, 66, 80].

ments.

IV. SUMMARY

We employed the *ab initio* VS-IMSRG method, based on two sets of chiral $NN+3N$ interactions, *i.e.*, EM1.8/2.0 and $NN+3N(\text{lnl})$ interactions, to precisely predict and elucidate the shell evolution properties of P, Cl, and K isotopic chains. The low-lying spectra of neutron-rich odd- A P, Cl, and K isotopes were systematically investigated. We observed that different isotopes exhibit varied phenomena with the increase in neutron number. The ground state spin-parities acted as sensitive probes of nuclear wave functions, serving as effective tools for studying nuclear structures in isotopes far from stability. Initially, we demonstrated that the inclusion of three-nucleon forces significantly enhances the accuracy of energy spectrum calculations. Considering three-nucleon forces, our VS-IMSRG calculations successfully reproduce the low-lying states for the neutron-rich P, Cl, and K iso-

topes, particularly the evolution of the $3/2_1^+$ and $1/2_1^+$ states in these isotopes. Further calculations of ESPEs confirmed that these energy level shifts are predominantly driven by monopole interactions, leading to a reversal of the $\pi 0d_{3/2}$ and $\pi 1s_{1/2}$ orbits at approximately $N = 28$. Both three-nucleon and tensor forces play important roles in this process. Interestingly, available data for the P isotopic chain were limited. Our calculations indicated a possible energy level inversion in ^{43}P at $N = 28$; this requires further investigation.

We also conducted a detailed investigation of the spectral properties of odd-odd nuclei, which has significantly deepened our understanding of these isotopic chains and their behavior in regions far from stability. The results from these calculations exhibited a strong correlation with the limited experimental data, thereby confirming the validity of our computational approach. We also offered predictions for the energy spectra of $^{40,42,44,46}\text{P}$, ^{46}Cl , and ^{52}K , which would be attained in future experiments.

References

- [1] M. G. Mayer, *Phys. Rev.* **75**, 1969 (1949)
- [2] O. Haxel, J. H. D. Jensen, and H. E. Suess, *Phys. Rev.* **75**, 1766 (1949)
- [3] B. Brown, *Prog. Part. Nucl. Phys.* **47**, 517 (2001)
- [4] O. Sorlin and M.-G. Porquet, *Prog. Part. Nucl. Phys.* **61**, 602 (2008)
- [5] A. Gade and T. Glasmacher, *Prog. Part. Nucl. Phys.* **60**, 161 (2008)
- [6] T. Otsuka, A. Gade, O. Sorlin *et al.*, *Rev. Mod. Phys.* **92**, 015002 (2020)
- [7] S. Sarkar and M. Saha Sarkar, *Phys. Rev. C* **81**, 064328 (2010)
- [8] F. Wienholtz, D. Beck, K. Blaum *et al.*, *Nature* **498**, 346 (2013)
- [9] E. Leistenschneider, M. P. Reiter, S. Ayet San Andrés *et al.*, *Phys. Rev. Lett.* **120**, 062503 (2018)
- [10] J. G. Li, *Phys. Lett. B* **840**, 137893 (2023)
- [11] J. G. Li, H. H. Li, S. Zhang *et al.*, *Phys. Lett. B* **846**, 138197 (2023)
- [12] W. F. Rogers, S. Garrett, A. Grovom *et al.*, *Phys. Rev. C* **92**, 034316 (2015)
- [13] E. Becheva, Y. Blumenfeld, E. Khan *et al.*, *Phys. Rev. Lett.* **96**, 012501 (2006)
- [14] D. Steppenbeck, S. Takeuchi, N. Aoi *et al.*, *Nature* **502**, 207 (2013)
- [15] J. G. Li, B. S. Hu, Q. Wu *et al.*, *Phys. Rev. C* **102**, 034302 (2020)
- [16] T. Nakamura, N. Kobayashi, Y. Kondo *et al.*, *Phys. Rev. Lett.* **112**, 142501 (2014)
- [17] I. Hamamoto, *Phys. Rev. C* **81**, 021304 (2010)
- [18] S. Bagchi, R. Kanungo, Y. K. Tanaka *et al.*, *Phys. Rev. Lett.* **124**, 222504 (2020)
- [19] N. Michel, J. G. Li, F. R. Xu *et al.*, *Phys. Rev. C* **101**, 031301 (2020)
- [20] H. L. Crawford, P. Fallon, A. O. Macchiavelli *et al.*, *Phys. Rev. Lett.* **122**, 052501 (2019)
- [21] E. Caurier, F. Nowacki, and A. Poves, *Phys. Rev. C* **90**, 014302 (2014)
- [22] P. Doornenbal, H. Scheit, S. Takeuchi *et al.*, *Phys. Rev. Lett.* **111**, 212502 (2013)
- [23] T. Otsuka, T. Suzuki, R. Fujimoto *et al.*, *Phys. Rev. Lett.* **95**, 232502 (2005)
- [24] T. Otsuka, T. Suzuki, M. Honma *et al.*, *Phys. Rev. Lett.* **104**, 012501 (2010)
- [25] N. A. Smirnova, K. Heyde, B. Bally *et al.*, *Phys. Rev. C* **86**, 034314 (2012)
- [26] M. Rosenbusch, P. Ascher, D. Atanasov *et al.*, *Phys. Rev. Lett.* **114**, 202501 (2015)
- [27] J. Fridmann, I. Wiedenhöver, A. Gade *et al.*, *Nature* **435**, 922 (2005)
- [28] Y. Sun, A. Obertelli, P. Doornenbal *et al.*, *Phys. Lett. B* **802**, 135215 (2020)
- [29] J. Papuga, M. L. Bissell, K. Kreim *et al.*, *Phys. Rev. Lett.* **110**, 172503 (2013)
- [30] J. Bjerregaard, O. Hansen, O. Nathan *et al.*, *Phys. Lett. B* **24**, 568 (1967)
- [31] E. Newman and J. Hiebert, *Nucl. Phys. A* **110**, 366 (1968)
- [32] F. Touchard, P. Guimbal, S. Büttgenbach *et al.*, *Phys. Lett. B* **108**, 169 (1982)
- [33] F. Nowacki and A. Poves, *Phys. Rev. C* **79**, 014310 (2009)
- [34] E. Caurier, G. Martínez-Pinedo, F. Nowacki *et al.*, *Rev. Mod. Phys.* **77**, 427 (2005)
- [35] S. R. Stroberg, A. Gade, T. Baugher *et al.*, *Phys. Rev. C* **86**, 024321 (2012)
- [36] B. D. Linh, A. Corsi, A. Gillibert *et al.*, *Phys. Rev. C* **104**, 044331 (2021)
- [37] R. Broda, J. Wrzesiński, A. Gadea *et al.*, *Phys. Rev. C* **82**, 034319 (2010)
- [38] V. Somà, P. Navrátil, F. Raimondi *et al.*, *Phys. Rev. C* **101**, 014318 (2020)
- [39] H. Hergert, S. Bogner, T. Morris *et al.*, *Phys. Rep.* **621**, 165 (2016)

- [40] S. R. Stroberg, H. Hergert, S. K. Bogner *et al.*, *Annu. Rev. Nucl. Part. Sci.* **69**, 307 (2019)
- [41] H. H. Li, Q. Yuan, J. G. Li *et al.*, *Phys. Rev. C* **107**, 014302 (2023)
- [42] Q. Yuan, J. Li, and H. Li, *Phys. Lett. B* **848**, 138331 (2024)
- [43] S. Michimasa, M. Kobayashi, Y. Kiyokawa *et al.*, *Phys. Rev. Lett.* **121**, 022506 (2018)
- [44] X. Xu, M. Wang, K. Blaum *et al.*, *Phys. Rev. C* **99**, 064303 (2019)
- [45] M. Mougeot, D. Atanasov, K. Blaum *et al.*, *Phys. Rev. Lett.* **120**, 232501 (2018)
- [46] K. Hebeler, S. K. Bogner, R. J. Furnstahl *et al.*, *Phys. Rev. C* **83**, 031301(R) (2011)
- [47] J. Simonis, K. Hebeler, J. D. Holt *et al.*, *Phys. Rev. C* **93**, 011302 (2016)
- [48] D. R. Entem and R. Machleidt, *Phys. Rev. C* **68**, 041001(R) (2003)
- [49] J. Simonis, S. R. Stroberg, K. Hebeler *et al.*, *Phys. Rev. C* **96**, 014303 (2017)
- [50] G. Hagen, A. Ekström, C. Forssén *et al.*, *Nature Phys.* **12**, 186 (2016)
- [51] R. F. Garcia Ruiz, M. L. Bissell, K. Blaum *et al.*, *Nature Phys.* **12**, 594 (2016)
- [52] T. D. Morris, N. M. Paruchowski, and S. K. Bogner, *Phys. Rev. C* **92**, 034331 (2015)
- [53] S. R. Stroberg, A. Calci, H. Hergert *et al.*, *Phys. Rev. Lett.* **118**, 032502 (2017)
- [54] <https://github.com/ragnarstroberg/imsrg>
- [55] N. Shimizu, T. Mizusaki, Y. Utsuno *et al.*, *Comput. Phys. Commun.* **244**, 372 (2019)
- [56] C. Ogilvie, D. Barker, J. England *et al.*, *Nucl. Phys. A* **465**, 445 (1987)
- [57] <https://www.nndc.bnl.gov/ensdf/>
- [58] A. M. Hill, A. Gade, D. Bazin *et al.*, *Phys. Rev. C* **104**, 014305 (2021)
- [59] V. Tripathi, S. Bhattacharya, E. Rubino *et al.*, arXiv: 2311.11434 [nucl-ex]
- [60] O. Sorlin, Z. Dombrádi, D. Sohler *et al.*, *Eur. Phys. J. A* **22**, 173 (2004)
- [61] S. Szilner, L. Corradi, F. Haas *et al.*, *Phys. Rev. C* **87**, 054322 (2013)
- [62] J. L. Yntema, *Phys. Rev. C* **4**, 1621 (1971)
- [63] J. Papuga, M. L. Bissell, K. Kreim *et al.*, *Phys. Rev. C* **90**, 034321 (2014)
- [64] X. Liang, R. Chapman, F. Haas *et al.*, *Phys. Rev. C* **66**, 037301 (2002)
- [65] J. Ollier, R. Chapman, X. Liang *et al.*, *Phys. Rev. C* **67**, 024302 (2003)
- [66] J. A. Winger, H. H. Yousif, W. C. Ma *et al.*, APS Southeastern Section Meeting Abstracts, AA.05 (1998)
- [67] F. Perrot, F. Maréchal, C. Jollet *et al.*, *Phys. Rev. C* **74**, 014313 (2006)
- [68] A. Huck, G. Klotz, A. Knipper *et al.*, *Phys. Rev. C* **21**, 712 (1980)
- [69] L. Weissman, O. Arnd, U. Bergmann *et al.*, *Phys. Rev. C* **70**, 024304 (2004)
- [70] N. Smirnova, B. Bally, K. Heyde *et al.*, *Phys. Lett. B* **686**, 109 (2010)
- [71] Y. Utsuno, *Physics* **4**, 185 (2022)
- [72] V. Somà, T. Duguet, and C. Barbieri, *Phys. Rev. C* **84**, 064317 (2011)
- [73] J. A. Winger, P. F. Mantica, and R. M. Ronningen, *Phys. Rev. C* **73**, 044318 (2006)
- [74] G. Burgunder, O. Sorlin, F. Nowacki *et al.*, *Phys. Rev. Lett.* **112**, 042502 (2014)
- [75] M. Sun, Y. Yu, X. Wang *et al.*, *Chin. Phys. C* **48**, 034002 (2024)
- [76] A. Huck, G. Klotz, A. Knipper *et al.*, *Phys. Rev. C* **18**, 1803 (1978)
- [77] P. A. Mandò, G. Poggi, G. L. Bianco *et al.*, *Phys. Rev. C* **21**, 2135 (1980)
- [78] S. Angelo, A. A. Pilt, and J. A. Kuehner, *Phys. Rev. C* **22**, 427 (1980)
- [79] W. Królas, R. Broda, B. Fornal *et al.*, *Phys. Rev. C* **84**, 064301 (2011)
- [80] A. Gade, B. A. Brown, D. Bazin *et al.*, *Phys. Rev. C* **74**, 034322 (2006)